# The Cross-Slope Transport of Momentum by Internal Waves Generated by Alongslope Currents over Topography

S. A. THORPE

*Department of Oceanography, University of Southampton, Southampton, United Kingdom*

(Manuscript received 13 February 1995, in final form 27 June 1995)

ABSTRACT

The alongslope currents flowing over topography of sufficiently small length scale, typically less than 10 km, on the continental slopes generate internal lee waves. These carry their momentum predominently toward shallower water, that is up the slope toward and across the shelf break, and onto the continental shelf, at least when, in summer, stratification permits their propagation. Analytical results show that even when the lee waves are generated with a component of their group velocity directed toward deeper water, reflection at the sloping seabed may lead to a turning toward shallower water. A numerical model is used to examine internal wave propagation and to quantify the flux of their momentum across the shelf break. In the conditions considered here with $f/N \ll 1$ and slope angle, $\alpha$, near 5 deg, the flux is parameterized by a stress (momentum flux per unit vertical area along the shelf break) per unit length downslope, $\tau_*$, given by

$$\tau_* = k\rho_0 VNh^2 \cos^4(\beta + \beta_0),$$

where $\rho_0$ is the mean water density, $V$ is the mean alongslope flow over the slope, $N$ is the buoyancy frequency in the vicinity of the shelf break, $f$ is the Coriolis parameter, and $h^2$ and $\beta$ are the mean square amplitude of the topography of wavenumber $l$, such that $Vl/N < 1$, and its mean orientation relative to the upslope direction, respectively. The constant $\beta_0$ is $7 \pm 2$ deg, and the formula is only valid if $\beta < 60$ deg. A value of $k$ of about $9\ (\pm 4) \times 10^{-6}\ \mathrm{m}^{-2}$ is suggested, with values near $1.3 \times 10^{-5}\ \mathrm{m}^{-2}$ when the topography is dominated by wavelengths less than $4\pi V/N$, or $5 \times 10^{-6}\ \mathrm{m}^{-2}$ when they exceed $20V/N$. This flux represents a transfer of momentum to the shelf currents in a direction contrary to the current over the slope that generates the internal waves. The magnitude of the flux is usually dominated by conditions near the top of the continental slope. Timescales of about 5 days are associated with this transfer on 5 deg slopes with 10-m high topography when $N \approx 10^{-2}\ \mathrm{s}^{-1}$.

## 1. Introduction

Internal waves generated by an alongslope flow of a stratified fluid of infinite depth over the rough topography of a continental slope have been shown to have a bias to propagate toward shallower water (Thorpe 1992). In the ocean where water is of finite depth, waves generated on the slope have a vertical structure that is modified by their reflections at the surface and the sloping seabed. The consequences are considered here, and a numerical model is used to provide an estimate of the horizontal flux of alongslope directed momentum carried across the shelf break by the internal waves, momentum which may modify the currents on the shelf. In the ocean the flux of momentum across the shelf break will also be influenced by other effects such as the internal lee waves resulting from tidal flows across the shelf break (Maxworthy 1979). The objectives here are to obtain measures of the flux produced by the alongslope flow interaction with topography, which may be compared with estimates of the contributions to the net flux from other sources, and to suggest a parametric form of the wave momentum flux that might be used in numerical models of the shelf sea circulation.

*Corresponding author address:* Dr. Steve A. Thorpe, Department of Oceanography, The University, Highfield, Southampton S09 5NH United Kingdom.

## 2. Analytical results

### *a. The generation of internal lee waves on a slope*

Thorpe (1992) considers the generation of internal waves by a uniform and steady flow, $V$, of an infinitely deep fluid with constant buoyancy frequency $N$, parallel to the mean isobaths of a uniform slope, which is tilted at angle $\alpha$ to the horizontal and covered by corrugations of wavelength $\lambda = 2\pi/l$ running up the slope at an angle $\beta$ to the line of maximum slope (Fig. 1). The condition for stationary lee waves to be generated is that

$$[ps_\alpha^2 + (1 - p)c_\beta^{-2}]^{1/2} < \chi < c_\beta^{-1}, \qquad (1)$$

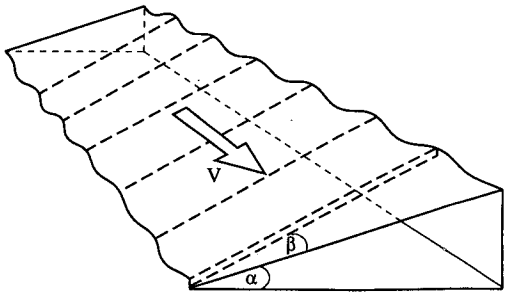


FIG. 1. The analytical model geometry. The mean flow, $V$, is uniform along a slope at an angle, $\alpha$, to the horizontal. The slope is covered with sinusoidal ripples with crests inclined at angle $\beta$ to the line of steepest ascent up the slope.

where $\chi = Vl/N$ is a Froude number of the flow and $p = 1 - (f/N)^2$; here $c_\beta = \cos\beta$, etc. Equation (1) may be written $2\pi V/N < \lambda_y < 2\pi V/(N[ps_\alpha^2 + (1 - p)c_\beta^{-2}]^{1/2})$, where $\lambda_y$ is the wavelength of the topography measured along the slope, the $y$ direction. This implies that, even though $N$ may be small in deep water, the values of $\lambda_y$ for which internal waves will be generated in the ocean are generally limited to scales between about 100 m and 10 km. Waves generated near the upper part of the slope are later found to be generally the most effective in the transport of momentum. There the Burger number, $B = NH/fL$, where $H$ is the water depth, is large, and generally it is justified to take $(f/N)^2 \ll s_\alpha^2 \ll 1$. For the present study the effect of the earth's rotation on the generation and propagation of the waves is neglected. Then (1) becomes

$$s_\alpha < \chi < c_\beta^{-1}. \tag{2}$$

Figure 2 shows the curves $\chi = s_\alpha$ and $\chi = c_\beta^{-1}$ between which conditions are favorable for the generation of internal waves. Although the wave phase is stationary in the flow, wave energy propagates with a positive component of group velocity toward shallow water when

$$-|\cos^{-1}(s_\alpha/\chi)| < \beta < \beta_{\text{crit}} = |\cos^{-1}[(1 - s_\alpha^2/\chi^2)^{1/2}/c_\alpha]|, \tag{3}$$

where $\beta_{\text{crit}}$ is the positive root of $c_\beta c_\alpha = (1 - s_\alpha^2/\chi^2)^{1/2}$. The stippled area of the $\chi-\beta$ plane (Fig. 2) shows this range; there is a preference for propagation toward shallow water for moderate values of $\beta$. This bias increases as $\chi$ decreases from $c_\beta^{-1}$ (when $\beta_{\text{crit}} = 0$) to $s_\alpha$ (when $\beta_{\text{crit}} = \pi/2$ and all waves generated with stationary phase travel toward shallow water whatever the value of $\beta$). When $\beta = 0$, the horizontal

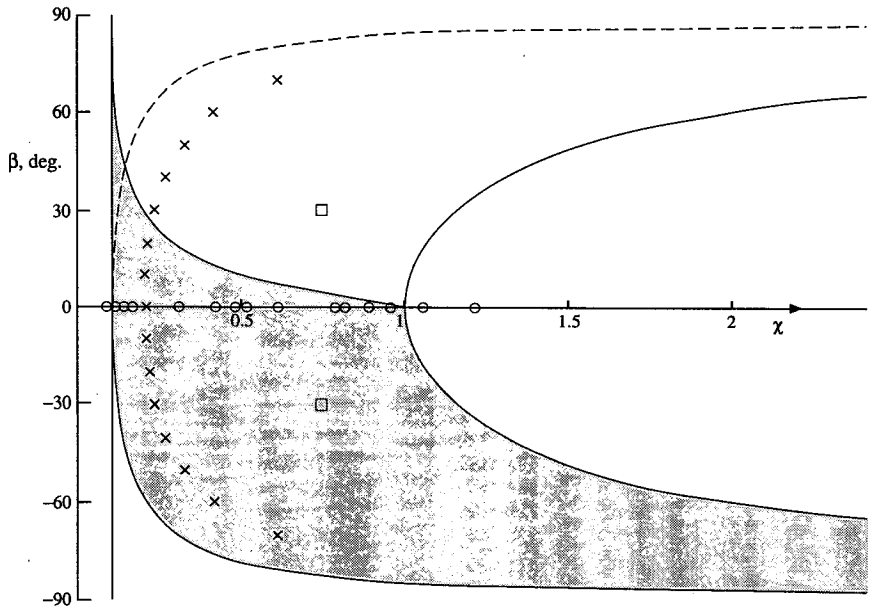


FIG. 2. The $\beta-\chi$ plane for $\sin^{-1}\alpha = 0.1$ showing the areas, $s_\alpha < \chi < c_\beta^{-1}$, in which stationary phase waves can be formed over sinusoidal topography on a slope. The direction of group propagation of these waves when generated is toward shallow water in the stippled area bounded above by the curve $\beta = \beta_{\text{crit}} = \cos^{-1}[(1 - s_\alpha^2/\chi^2)^{1/2}/c_\alpha]$ and below by $\chi = s_\alpha/c_\beta$. All waves in the sector between $\chi = s_\alpha/c_\beta$, the dashed line, and $\chi = c_\beta^{-1}$ will eventually propagate toward shallower water depths (after sufficient reflections if $\beta > 0$; see section 2b). Squares, crosses, and circles correspond to the parameter values at which numerical experiments shown in Figs. 5, 6, and 7 are made, respectively.

component of the group velocity directed toward shallow water is

$$c_{gX} = Vs_\alpha(1 - \chi^2)^{3/2}(\chi^2 - s_\alpha)^{1/2}/\chi^2 c_\alpha^2. \quad (4)$$

The angle between the projection of the internal wave group velocity vector in a frame of reference moving with the mean flow onto the horizontal plane and a horizontal direction normal to the isobaths, $\phi$, is given by

$$\cos\phi = [s_\alpha c_\alpha - t_\beta(t_\theta^2 c_\alpha^2 + t_\theta^2 t_\beta^2 - s_\alpha^2)^{1/2}]/[t_\theta(c_\alpha^2 + t_\beta^2)] \quad (5)$$

(see Eriksen 1982). Here $\theta = \sin^{-1}(\chi c_\beta)$, the angle made by the group velocity of the internal waves, again as seen in the moving frame of reference, to the horizontal. The group velocity vector viewed in a fixed frame of reference has a corresponding direction, $\Phi$, given by

$$\tan\Phi = \tan\phi - 2/(\sin 2\phi \cos^2\theta). \quad (6)$$

This angle is that which the constant phase surfaces at the sea surface make with the line of the slope break, a direction made visible in satellite photographs of the internal wave patterns on sea surface.

### b. *The effect of the upper boundary*

Reflection of waves from a smooth sea surface or from a smooth slope will preserve the wave frequency and alongslope wavenumber, and waves will therefore remain stationary in the alongslope flow. Large surface current fluctuations are generated by internal waves when $\beta$ is close to $-|\cos^{-1}(s_\alpha/\chi)|$, where the propagation direction changes from being toward shallow water to being toward deep (Thorpe 1992). After downward reflection at the sea surface, waves will return to the seabed with constant phase planes meeting the slope at an angle $\beta_1$ to the line of steepest slope (i.e., $\beta_1$, like $\beta$, is measured from the line of greatest slope) given by

$$\tan\beta_1 = -[c_\alpha/t_\phi + s_\alpha/(t_\theta s_\phi)], \quad (7)$$

an angle which decreases toward $-90$ deg on each subsequent reflection. Provided that $\theta > \alpha$, the angle $\phi$ will decrease toward zero every time the waves are reflected from the slope, even if the internal waves are first generated with a positive component of their group velocity directed toward deeper water (see Eriksen 1982, Fig. 2b). The internal lee waves are therefore trapped within the slope-shelf region when $\theta > \alpha$, their group velocity relative to the mean flow progressively turning toward the upslope direction on each reflection from the bottom. The only waves that may escape will be either those generated with a component of group velocity toward deeper water, the areas of wave generation but which are not stippled in Fig. 2, or those which, on generation, propagate toward shallow water but have $\theta < \alpha$ (those in the area in Fig. 2 with $\beta > 0$ and $s_\alpha < \chi < s_\alpha/c_\beta$). The latter reflect toward deeper water on their first reflection from the slope. Of the former there are two classes: first, those that propagate at an angle below the horizontal, which may not intersect the slope, and, second, those, which after their first reflection from the sea surface or on a subsequent reflection while still having a positive component of group velocity toward deeper water, reach the abyssal plain. Some waves generated sufficiently near the foot of the slope will always "escape" in this way. Over the area in the $\chi$–$\beta$ plane in Fig. 2 in which $s_\alpha/c_\beta < \chi < c_\beta^{-1}$ all stationary phase waves, including those that are propagating toward deeper water when generated (provided they reflect sufficiently often from the slope and do not reach the abyssal plain), will eventually propagate toward shallower water depths. The slope acts to trap and direct the internal waves toward the shelf break.

The condition that internal waves generated at a distance $L$ measured down a slope from the shelf break where the water depth is $H$ shall reach the shelf break before reflecting from the seabed is that

$$L < L_{\text{crit}} = 2Hc_\phi/[c_\alpha(t_\theta - t_\alpha c_\phi)], \quad (8)$$

which is small in comparison with the typical extent of continental slopes. Most waves generated on the slope will suffer multiple reflections at the slope and sea surface before reaching the shelf break unless their generation point is close by.

### c. *Effects of nonuniform N and α*

The conclusions of section 2b ignore the variations of $N$ and $\alpha$ that occur in the ocean. Waves propagating upward toward the sea surface from the lower parts of the slope will encounter regions where the density gradient and therefore $N$ increases. Since the intrinsic frequency, $\sigma$, is conserved, the angle of the relative group velocity vector to the horizontal, $\theta = \sin^{-1}(\sigma/N)$, decreases as $N$ increases, and the wave paths will be refracted toward the horizontal. The waves propagating toward shallower water may therefore return to meet the slope propagating at a smaller angle, $\theta$, than the local slope and will then be reflected back toward deeper water. Waves propagating toward deeper water at generation may never reach the surface and will therefore not be reflected back to the slope but continue to radiate into deeper water and will not be trapped in the shelf region.

In contrast, when the depth of the winter convectively mixed layer exceeds that of the continental shelf or in other conditions in which $N$ becomes very small below the depth of the shelf break, internal waves will be unable to propagate beyond the level at which $\sigma = N$. They will instead be reflected down to be trapped

in the wedge between the slope and the level at which $\sigma = N$. Unless dissipated in the course of propagation, their amplitude will grow (Wunsch 1971) and they will break, contributing to the local deepening of the convective layer if dissipation is not sufficient to limit them. No momentum will then be carried by the waves onto the shelf.

## 3. The numerical model

The semispectral hydrostatic primitive equation model (SPEM) developed by Haidvogel and others (see Haidvogel et al. 1991) is used to examine stratified uniform flow along a channel with a section consisting of a constant depth shelf, slope, and constant depth abyssal plain (Fig. 3). The governing nonlinear momentum, density, and continuity equations described by Chapman and Haidvogel (1993: but omitting the Coriolis force) are integrated. The uniform flow runs parallel to the isobaths of the slope and is laterally constrained by parallel vertical boundaries on the shelf and abyssal plain. Periodic conditions are chosen in the alongslope direction. The vertical flow structure is represented through modified Chebyshev polynomials, seven being found adequate when the buoyancy frequency $N$ of the fluid is constant in depth, but 21 are found necessary to satisfactorily resolve the flow in some runs in which $N$ varies with depth (section 4c). Experiments are made with uniform and oscillatory flows over topography of various kinds on the slope.

Like Chapman and Haidvogel a free slip boundary condition at the lower and upper (rigid lid) boundary is adopted. The effects of wave scattering by surface roughness (see Baines 1971a,b) or those of a turbulent or mixed boundary layers on the generation of internal lee waves are disregarded; no attempt is made here to represent their presence by the introduction of viscous boundary conditions on the seabed. In reality these turbulent layers may reduce the effective amplitude of the topography by some presently unknown factor. Where necessary, higher viscosity sponge layers are introduced in the vicinity of the lateral boundaries to prevent their affecting the flow over the slope.

The $e$-folding damping time of a first-mode internal wave of horizontal wavenumber $k$ in water of shelf depth $H$ is $\nu_h^{-1}k^{-2}$, where $N$ is the uniform buoyancy frequency and $\nu_h$ is the horizontal viscosity (see Thorpe 1968). For $\nu_h = 1$ m$^2$ s$^{-1}$, $H = 200$ m, and a horizontal wavelength of 1.86 km, this is a damping time of 24.3 h, a period in which the waves will propagate onto the shelf at their group velocity (0.059 m s$^{-1}$) a distance of only 5.2 km. The fluxes of momentum, proportional to $a^2$, decay twice as fast. This is consistent with the damping of first-mode internal waves on the shelf, which are found in model runs with a harmonic damping coefficient along sigma coordinates, $\nu_\sigma = 1$ m$^2$ s$^{-1}$. Runs with reduced deep water depth, effectively reducing the downslope length of the slope, show that with $\nu_\sigma = 1$ m$^2$ s$^{-1}$, the momentum flux across the shelf break is predominently from the upper 2–4 km, waves from greater depths being greatly damped. An "acceptable" value of $\nu_\sigma$, say 0.1 m$^2$ s$^{-1}$, which might allow internal waves to propagate from the foot of the slope to the shelf break and also allow run times of several tidal periods, does not, however, give much greater model stability than zero viscosity; both the run time before instability and momentum fluxes are similar, suggesting that the effect of "start up" transients is negligible. The horizontal viscosity is therefore set as zero in all subsequent runs.

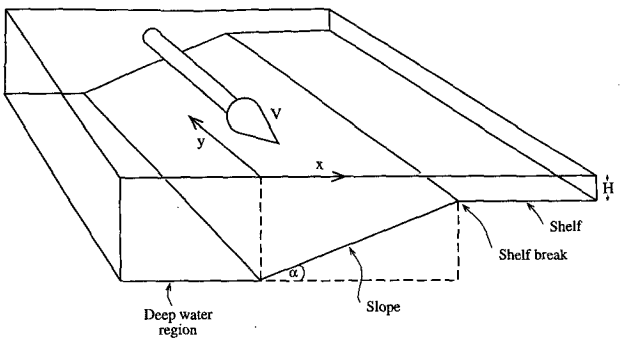


FIG. 3. Sketch of the numerical model geometry. The deep water region is generally taken to be 1000 m deep and the shelf 200 m deep. Both are bounded by vertical walls (or by "spongey layers" to absorb wave energy). Topography is superimposed on the slope. The model is periodic in the alongslope direction. The mean flow is parallel to the line of the shelf break and uniform across the channel formed between the side walls.

Numerical instability proves to be unavoidable with zero viscosity, but may be delayed until steady conditions are reached. Instability is commonly preceeded by a well-defined fall and then a huge and rapid rise in momentum flux, accompanied by the appearance of structure at, or close to, the limit of resolution in velocity and density plots. A procedure adopted once the dependence of fluxes on the amplitude of the topography, $a$, had been established is to make runs with smaller amplitude topography and "scale up." This allows much longer runs to be made before instability sets in, but imposes an effective constraint of being able to examine only "linear" effects and not, for example, the second-order effects of reflected wave scattering over large topography.

"Typical" values of quantities such as slope angle, flow, etc., appropriate to characterize the ocean, are selected with the approach that, once insight is obtained into the understanding of momentum flux, variation or sensitivity to local or more realistic values may be examined. Most of the runs are made with standard parameters of alongslope topographic wavelength $\lambda_y = 3$ km and a slope angle, $\alpha = 5.74$ deg such that $\sin\alpha = 0.1$. This angle is much larger than is generally char-

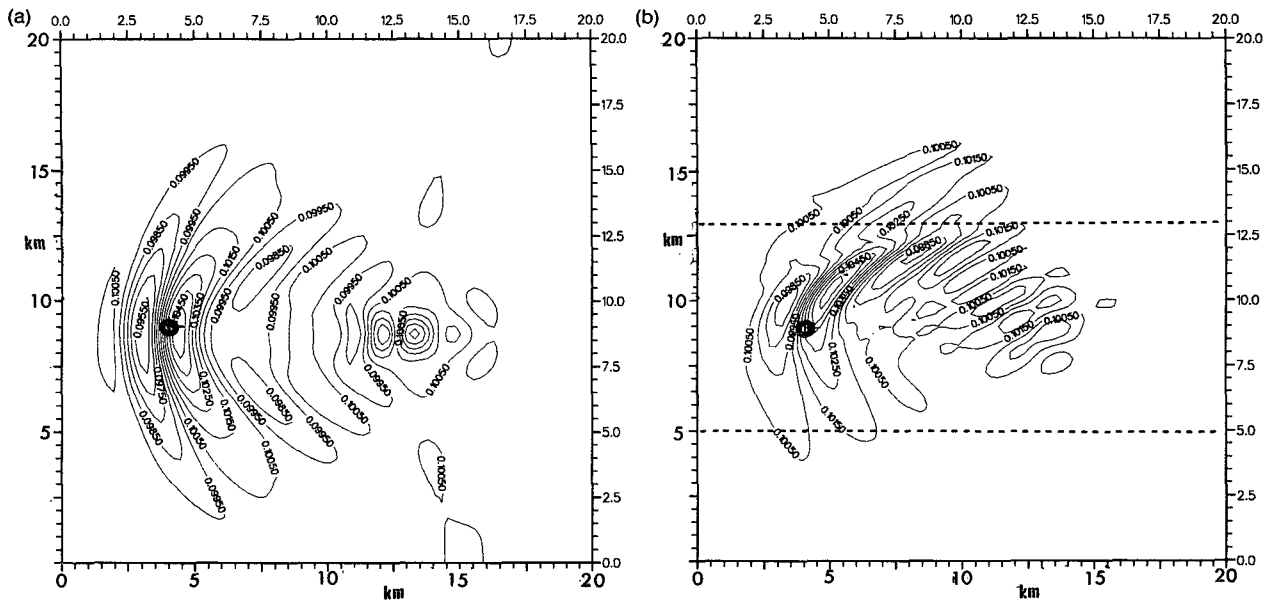


FIG. 4. The effect of the slope on the perturbation field caused by an alongslope flow over an isolated Gaussian "bump" 10 m high with scale radius 2.1 km at the position marked with a circle. Here $N = 10^{-3}$ s$^{-1}$ and the flow $V = 0.1$ m s$^{-1}$ is to the right. The scales are in km. (a) The alongslope component of the current field at the sea surface 30 h after the onset of the flow, with zero slope angle and 600-m uniform water depth. The perturbation near $x = 9$ km, $y = -13$ km is a result of the downstream advection of the initial disturbance over the topography when the flow is started. (b) The same current component at the same time with the topography still located at 600-m water depth, but now halfway up a uniform slope. The slope has $s_\alpha = 0.1$ and lies between the dashed lines marking the edges of the 200-m "shelf" (at the top) and the 1000-m deep plain (at the bottom of the figure). In both figures contours are shown at 0.05 cm s$^{-1}$ intervals. The largest current component fluctuation from the mean 10 cm s$^{-1}$ current is 0.45 cm s$^{-1}$. The effect of the slope is to distort the wave pattern in the upslope direction toward and across the shelf break.

acteristic of the whole slope but is typical of upper slopes, which are likely to have the greatest effect on the transport across the shelf break (see section 6). The downslope extent is taken to be 7.8 km so that the water at the foot of the slope is 1 km deep; $N = 10^{-3}$ s$^{-1}$ and the alongslope flow $V = 0.1$ m s$^{-1}$.

The analytical results (section 2) provide a guide to the wave patterns to be reproduced in the model. With the selected parameter values and $\beta = 0$, the value of $\chi$, $= Vl/N$, is 0.21, which is in the range of values (2) for which lee waves will be generated. The angle $\beta$ is less than $\beta_{\text{crit}} = 27.9$ deg (from 3), and waves propagate toward shallow water at a group speed $c_{gX} = 0.044$ m s$^{-1}$ (from 4), therefore taking about 50 h to reach the shelf break from the foot of the slope. Other derived values are $\phi = \cos^{-1}(t_\alpha/t_\theta) = 62.2$ deg (from 5) and $\Phi = -32.6$ deg (from 6). The waves would reflect from the sea surface to meet the slope again along a constant phase line of inclination $\beta_1 = -46.4$ deg (from 7). Here $L_{\text{crit}}$ is equal to 1.13 km (from 8) if $H = 200$ m so that only a very short length of slope generates waves that may completely avoid momentum reduction from bottom reflection before reaching the shelf break. The values are sensitive to $\beta$ variation; corresponding values when $\beta = 20$ deg (or $-20$ deg) are $\theta = 11.4$ (11.4) deg, $\phi = 82.1$ (41.0) deg, $\Phi = -23.6$ ($-50.8$) deg, $\beta_1 = -32.6$ ($-61.6$) deg, and $L_{\text{crit}} = 0.29$ (2.37) km, respectively.

Stationary internal waves of the dominant first mode on the shelf, produced by periodic topography at the shelf break of wavenumber $l$, travel at an angle $\psi$ to the alongslope direction with speed through the water $c = V\cos\psi$, the condition of stationary phase, where

$$\cos\psi = lH(1 - \chi^2 c_\beta^2)^{1/2}/(\pi\chi), \qquad (9)$$

and have group velocity normal to the slope

$$c_{gn} = V\cos\psi(1 - \chi^2 c_\beta^2). \qquad (10)$$

With the values of $V$, $H$, etc., used above, $\psi = 51.6$ deg and $c_{gn} = 0.059$ m s$^{-1}$. The wavelength of the waves is $\lambda_y \cos\psi$ or 1.86 km.

## 4. Model results

### a. *Steady flow over "bump" topography*

The numerical code was tested for its ability to reproduce earlier results of Chapman and Haidvogel (1993) for stratified flow around isolated Gaussian topography on a horizontal plane. A slope was then introduced. Figure 4 shows one example of the effect this has on the perturbation field caused by an alongslope

flow with $N = 10^{-3}$ s$^{-1}$ and speed $V = 0.1$ m s$^{-1}$ over an isolated Gaussian "bump" 10 m high with scale radius 2.1 km at the position marked with a circle. The model grid is 0.25 km × 0.25 km. Shown is the alongslope component of the current field at the sea surface 30 h after the onset of the flow, when (a) the slope angle is zero and the water depth is 600 m and (b) when the topography is located at 600-m water depth, halfway up a uniform slope with $s_\alpha = 0.1$ between the 200-m "shelf" and the 1000-m deep plain. The wave pattern is distorted with propagation toward the upslope direction. The momentum flux across the 20-km-long shelf break, $Fx_1$, is given by $Fx_1/\rho_0 VN = 1.55 \times 10^4$ m$^3$, and this is about six times greater than the momentum flux across the foot of the slope at the same time.

### b. *Steady flow over sinusoidal topography*

Further tests of the model were made to test whether the internal waves generated over sinusoidal ripples on the slope in the early stages of the flow (times of 3–12 h) were consistent with predictions. The inclinations of the waves to the horizontal and to the shelf break, were in accord with the predictions of section 2. Figure 5 shows examples of waves generated with propagation toward and away from deeper water at values of $\chi$ and $\beta$ marked by squares in Fig. 2. Particularly notable in both cases are the intensification of the perturbations near the top of the slope and the set of waves advancing across the shelf at speeds that accord with (10), both when the generation is toward and away from shallow water.

Runs were made to explore the properties of the model with the "typical" values and sinusoidal rippled topography of amplitude $a$. Seven polynomials were usually taken to define the vertical structure, and an alongslope grid of 14 points and an upslope direction grid of 101 points was generally used. Values of the momentum flux through a vertical plane at the shelf break, $Fx_1$, generally increases monotonically with time after the flow is switched on, before settling to a steady value about which fluctuations of 5%–10% occur after a "spinup" time estimated to be approximately equal to that required for waves to arrive from the foot of the slope (i.e., about 50 h for the "typical" values). Numerical instability is usually delayed until the model has run for some 90 h. Six runs made with "typical" values and with $a$ ranging from 0.5 m to 15 m, show that both the growing and steady values of $Fx_1$ scale with $a^2$, as expected by linear theory, up to values of $al = 0.024$; that is, up to $a = 11.5$ m. Smaller values of $Fx_1$ are found at larger $a$. Subsequent runs with more realistic topography, section 4d, confirm this $a^2$ scaling during the early stages of spinup.

Figure 6 shows the variation of a scaled steady flux at the shelf break, $F_1 = Fx_1/(a^2\rho_0 VNA)$, where $\rho_0$ is the mean (reference) density and $A$ is the area of the vertical section at the shelf break, for various values of $\beta$ and with $V = 0.1$ m s$^{-1}$, $a = 0.5$ m, $\lambda_y = 3$ km, and $N = 1 \times 10^{-3}$ s$^{-1}$. The corresponding $\chi$ and $\beta$ values are shown by crosses in Fig. 2. Values of $Fx_1$ are factors of 3.4 (±1.1) greater than those found for $|\beta| < 40$ deg when $\nu_\sigma = 1$ m$^2$ s$^{-1}$, demonstrating the expectedly large wave damping produced by viscosity when it is included in the numerical model, as discussed in section 3. Slightly higher fluxes are found for $\beta < 0$ than at the corresponding positive values of $\beta$, as expected from the analytical results. The data are well fitted by $F_1 = F_{10}\cos^q(\beta + \beta_1)$ with $q = 3.9 \pm 0.15$ and $\beta_1 = 7 \pm 2$ deg. The figure also shows the scaled horizontal momentum flux through a vertical plane at the foot of the slope, $F_2$. The analytical model with infinite depth predicts that the direction of the wave flux changes at $\beta = \beta_{\text{crit}} = 27.9$ deg. Indeed, $F_2$ is negligible for $\beta < \beta_{\text{crit}}$ when all wave propagation at generation is predicted to be toward shallow water. For larger $\beta$, $F_2$ increases, becoming equal to $F_1$ at $\beta = 42$ deg and exceeding $F_1$ at larger $\beta$. However, $F_1$ does not approach zero as $\beta$ increases toward $\beta_{\text{crit}}$. This is in accordance with the earlier conclusion that even when the group velocity of the generated waves has a positive component toward deeper water, reflections from the seabed will lead to momentum transfer toward shallow water.

Figure 7 shows the variation of the scaled flux, $F_1$, with $\chi$, when $\beta = 0$ and with $a = 0.5$ m. Here $V$ takes values from 0.07 to 0.2 m s$^{-1}$, $N$ values from 0.5 to 2 ($\times 10^{-3}$ s$^{-1}$), and $\lambda_y$ values from 0.5 to 6 km. The corresponding values of $\chi$ are shown by circles in Fig. 2. The mean flux is estimated between 48 and 84 h after the onset of the flow. Near the bounding values of $\chi$ for wave generation, for example at values of $\chi = 0.105$ (close to $\chi = s_\alpha$, when waves propagate with $\theta$ close to $\alpha$), and 0.90 and 0.97 (near $\chi = c_\beta^{-1}$ when $\theta$ is close to $\pi/2$), the values of $F_1$ are unsteady and still generally increasing when numerical instability sets in. These points are not shown in the figure. Very small values of flux are found when $\chi > 1$. The mean values of the scaled flux are about 0.035 m$^{-1}$, with a rise in values occurring near $\chi = 0.44$. At time $t$ such that $Nt = 64.8$ (18 h if $N = 10^{-3}$ s$^{-1}$), $F_1$ has reached about half the "steady" value when $0.1 < \chi < 0.3$, but is already within the uncertainty of the "steady" values when $0.5 < \chi < 0.8$. Over the limited range of values tested, the scaling gives consistent results within the uncertainty of the variations of the estimates and is independent of $\lambda_y$ except in so far as it affects $\chi$. As expected, the momentum flux into deep water at the foot of the slope is very small, but positive, for all values of $\chi$.

The effect of changing the slope angle has not been examined in detail. When $\chi = 0.21$ and $s_\alpha = 0.05$, but maintaining the same slope length so that the maximum

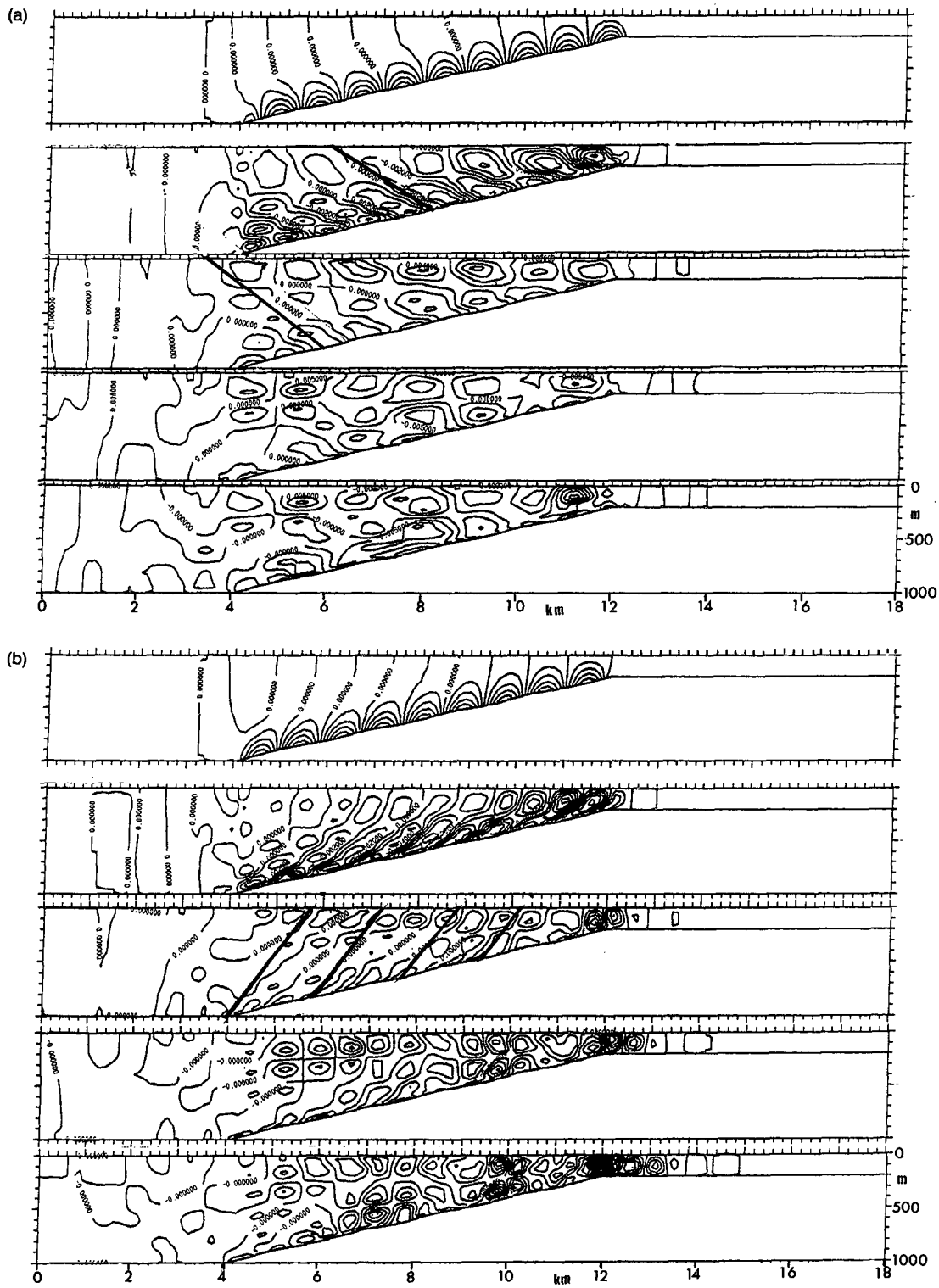


FIG. 5. Vertical sections along the line of steepest slope showing contours of the perturbation density field at (top to bottom) 0.6, 3, 6, 9, and 12 h after the onset of the 0.1 m $s^{-1}$ alongslope flow with $\lambda_y$ = 1 km and $N = 10^{-3}$ $s^{-1}$, when (a) $\beta$ = 30 deg, when the direction of the wave energy propagation is toward deeper water, and (b) $\beta = -30$ deg, when initial propagation is toward less deep water. The parameter $\chi$ = 0.73 in each case. The corresponding ($\chi$, $\beta$) points are marked as squares in Fig. 2. The heavy lines at 3 or 6 h indicate the direction of the constant phase surfaces predicted analytically.

water depth is 600 m, values of $F_1$ are 60% higher than those at $s_\alpha = 0.1$. The fluxes into deep water at the foot of the slope were also higher, but still small. When $s_\alpha = 0.2$, maintaining the maximum water depth at 1000 m and so shortening the slope, similar values of $F_1$ are found near $\chi = 0.3$, but values 50% lower than those shown in Fig. 7 when $\chi = 0.48$ and 0.62, suggesting that here at least the flux is proportional to the area of slope generating the waves. Thorpe (1992) showed that, in an infinitely deep fluid, the maximum upslope energy flux increases with $\alpha(<12.2°)$ but the maxima occur at different values of $\chi$ (and of $\beta$ when this angle is varied). The dependence of the momentum flux in limited depth may have a more complex relation to the angles and Froude number. We conclude, however, that the range of values obtained in Fig. 7 are representative of the momentum fluxes at other slope angles.

### c. *Oscillatory flow with nonuniform N over sinusoidal topography*

Four runs were made with oscillatory flow of frequency $\sigma = 2\pi/12$ h (representing tidal motion) over sinusoidal topography of wavelength 3 km with $\beta = 0$, with and without steady components, and with $N$ varying linearly from $10^{-2}$ s$^{-1}$ at the surface to $10^{-3}$ s$^{-1}$ at 1000 m. These case studies, described in the appendix, illustrate the effects of the variations in the time and position on the slope favoring wave generation, and in the refraction of wave propagation that will occur in the real ocean as the result of $N$ having a depth dependence. It is found that stratification and flow oscillation modify the area of the slope and the time over which wave generation is possible, and create an oscillatory flux phase lagged relative to that of the flow. Even a relatively small mean flow results in a rectified momentum flux of mean magnitude similar to those found in steady flows (section 4b); the mean fluxes are, however, not greatly changed by the presence of alongslope tidal currents.

### d. *Real topography*

An area of real topography on the continental slope between 150 and 500 m northwest of Ireland near the Barra Fan at 56° N, 10° W was chosen for study since this is the site of the Shelf Edge Study of the U.K. Land–Ocean Interaction Study (LOIS) planned for 1995–1997. The area is shown in Fig. 8. The mean bottom slope is about 5 deg, close to that adopted for the earlier modeling. The slope is marked by small topographic features that have resulted from local slumping. These have a relative rms amplitude, $h$, of 9.2 m found by taking average displacements in sections directed in the alongslope direction. There are no canyons or signs of feeder gullies for water cascading off the shelf following periods of winter cooling. The topography does contains some linear features (e.g., near $x = 0.5$–$2.5$ km, $y = -3.7$ km in Fig. 8) some 20 m in amplitude sloping at angle $\beta = -12$ deg (an angle which may not significantly alter the momentum flux from its $\beta = 0$ value; see Fig. 6), as well as undulations near $x = 2$ km, $y = -4$ to $-7$ km. The wavenumber spectrum of the alongslope roughness in the depth range from 150 m to 500 m has a slope close to $-1$ in the wavelength range from 600 m to 4 km. The mean current in the area is the "slope current" toward the north at about 0.1 m s$^{-1}$.

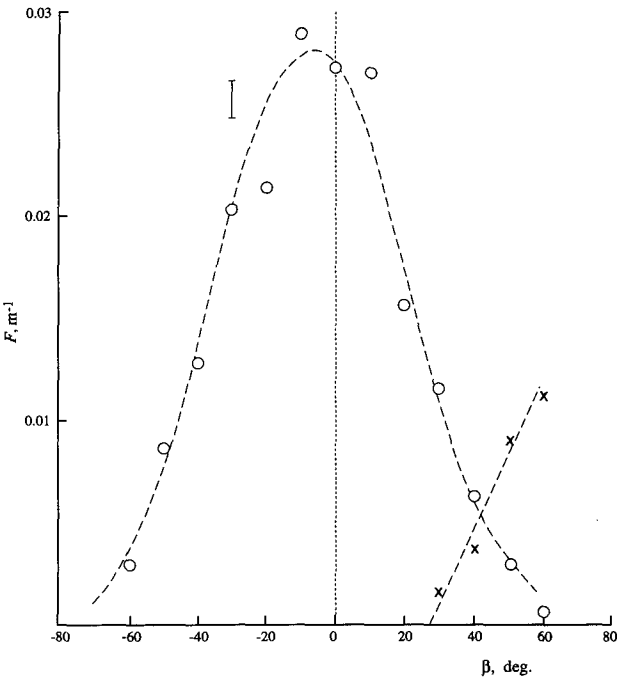


FIG. 6. Plot of steady values of the scaled horizontal flux of horizontal momentum, $F_1 = Fx_1/(a^2\rho_0 VNA)$ (circles) and $F_2 = Fx_2/(a^2\rho_0 VNA)$ (crosses) vs $\beta$, derived from the numerical model with "typical" values of $V = 0.1$ m s$^{-1}$, $\alpha = 5.74$ deg, $N = 10^{-3}$ s$^{-1}$. Larger values of the flux, $F_1$, are found at negative values of $\beta$ than at the corresponding positive values. $F_2$ is significantly greater than zero only when $\beta$ is greater than about 28 deg and dominates the flux from the slope when $\beta > 40$ deg. The dashed curve is $F_1 = 0.028 \cos^4(\beta + 7.0 \text{ deg})$.

For the purposes of modeling, the topography is made periodic by extending the 6 km × 6 km area along the slope, using linearly interpolated joining regions 1.5 km in length, so that the whole is periodic with wavelength 7.5 km. This exceeds the 6.3-km scale required to satisfy (2) with $V = 0.1$ m s$^{-1}$, $N = 10^{-3}$ s$^{-1}$, and $\beta = 0$, so should not then lead to significant wave generation.

The numerical model was run using a grid size of 200 m × 200 m and with $N = 10^{-3}$ s$^{-1}$. With full amplitude topography the model failed after only 6 h,

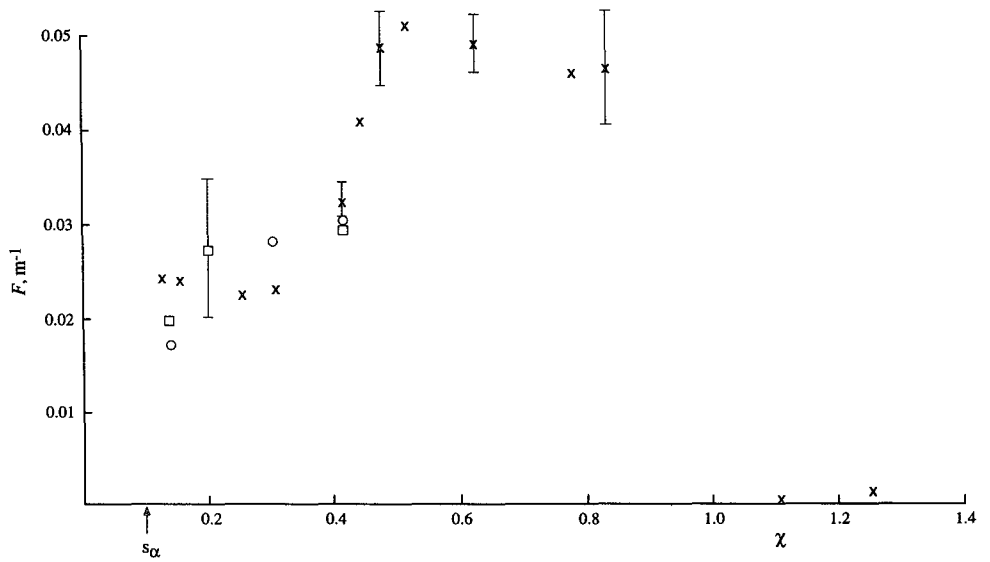


FIG. 7. Plot of steady values of the scaled horizontal flux of horizontal momentum across the shelf break, $F_1 = Fx_1/(a^2\rho_0 VNA)$, vs $\chi$ at $s_\alpha = 0.1$ and $\beta = 0$. The points represent variation of (crosses) $\lambda$, (circles) $U$, and (squares) $N$, from the "typical" values, $\lambda = 3$ km, $U = 0.1$ m s$^{-1}$, and $N = 1 \times 10^{-3}$ s$^{-1}$. The vertical bars represent the range of variability of the numerical estimates.

but it ran with 1/40 scale topography for 18 h before the onset of numerical instability. The momentum flux, $Fx_1$, at the shelf break, taken as the mean position of the 173.8-m depth contour, scales well with $h^2$ at all times prior to instability. Figure 9 shows sections of contours of current fluctuations resulting from a uniform current $V = 0.1$ m s$^{-1}$ flowing in the positive $y$ direction, approximately that of the real flow in the area, during a period of 15 h after the initiation of the flow. The development of waves and their propagation onto the shelf is seen in (a), the contours of the $x$ directed currents at the sea surface. Currents are linearly related to topographic scale. The current components found by scaling up the 1/40 scale model output have a maximum value of 4 cm s$^{-1}$ at 15 h. Figure 9b shows the initial tilt of the constant phase surfaces into the flow in a vertical section directed along the slope. The most pronounced features in the vertical section appear over the lee-facing slope of the linear topographic feature near $y = -3$ km.

Figure 10 shows the variation of the nondimensionalized upslope momentum flux $F = Fx/(h^2\rho_0 VNA)$, with time and depth, $z$. Here $Fx(z, t)$ is the mean upslope momentum flux at depth $z$ and time $t$, and $A$ is the area of the vertical section at the 173.8-m depth contour; $A$ (and $h$) are maintained at constant values so that the relative magnitude of the flux at different positions on the slope can be compared. At the foot of the slope, 500-m depth, the flux is small, directed toward deep water, and is steady to within 15% after 14 h. The flux at 442 m rises to a maximum after 10 h as waves from the lower parts of the slope arrive, before falling. The fluxes at 351 m and 272 m show similar patterns, but reach their maxima at successively later times. The flux at 174 m is relatively slow in growing, the maximum rate of increase not being reached until 12 h after the onset of flow, and the flux continues to increase until the onset of numerical instability between 18 and 19 h. As can be seen from Figs. 9a and 9b, the internal waves reaching the shallower depths come mainly from the area of rough topography at depth 250 to 350 m and therefore do not contribute to the momentum flux at shallower depths until they have propagated some distance upslope. The variations in the rate of growth of momentum at different levels naturally leads to periods of apparent flux convergence between the different vertical sections up the slope. At 18 h the fluxes show a monotonic increase from deep water to shallow. The value of $F_1$ at the shelf break, $Fx$ at $z = 174$ m, is 0.022 m$^{-1}$, a value which corresponds to the data used in constructing Fig. 8 with $\beta = 0$ after the same time period if $\chi$ is about 0.2 or $\lambda_x = 3.1$ km. The long-term value of $F_1$ inferred from Fig. 7 is 0.058($\pm$0.01) m$^{-1}$. The downslope length is, however, only some 5 km, compared with 8 km in the earlier model runs. The flux per unit slope area is therefore similar to the average values of the nondimensionalized upslope momentum flux $F_1 = Fx/(a^2\rho_0 VNA)$ in Fig. 7 with the amplitude $a$ of the rippled topography replaced by the rms height $h$.

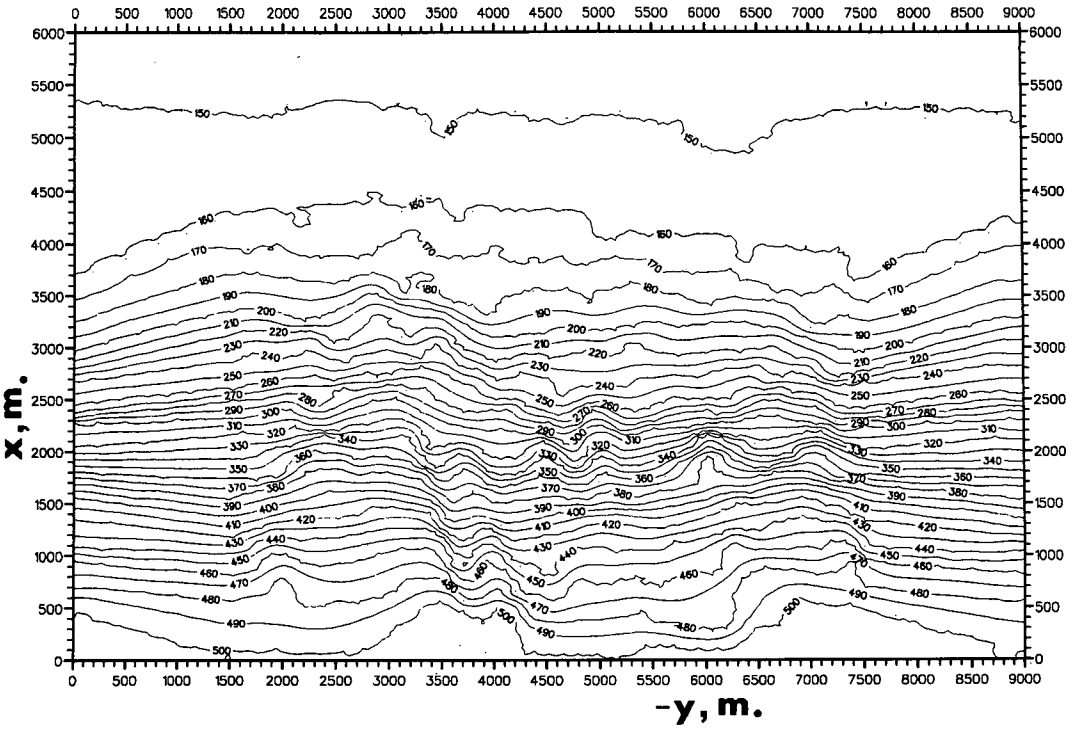


FIG. 8. Contours of the "real" topography on the edge of the Malin Shelf to the west of the United Kingdom. The topography taken from a detailed survey (Holmes 1994) is represented between 1600 m and 7400 m on the lower axis, with linear interpolation to give an alongslope periodicity of the topography used in the model of wavelength 7.4 km. The alongslope position of the true data 4500 m along the lower ($-y$) axis is at 56°26′N and 9°09′W, and the orientation of this axis is 200° to true north. The model domain is extended at 500-m depth for 1.4 km below this axis and for 1.4 km at the top of the slope with 150-m water depth, with a viscous "spongy layer" to dissipate the internal waves in the final 1 km.

## 5. A parametric representation of the stress

### *a. A working value for the flux across the shelf break*

The model results described above are consistent with a stress $\tau_*$ at the shelf break produced by waves generated per unit area of the slope given by

$$\tau_* = k\rho_0 VNh^2 \cos^4(\beta + \beta_0), \qquad (11)$$

where $\rho_0$ is the mean water density, $V$ is the mean alongslope flow over the slope, $N$ is the buoyancy frequency in the vicinity of the shelf break, and $h$ and $\beta$ are the rms amplitude of the topography of scale such that $\chi < 1$, and its mean orientation, respectively. The $\beta$ variation is derived from Fig. 6 with $\beta_0 = 7(\pm 2)$ deg and is valid only if $\beta < 60$ deg. The value $k$ determined from Fig. 7 is about $9 \times 10^{-6}$ m$^{-2}$, with values near $1.3 \times 10^{-5}$ m$^{-2}$ when the topography is dominated by wavelengths less than $4\pi V/N$ ($\chi > 0.5$), or $5 \times 10^{-6}$ m$^{-2}$ when they exceed $20V/N$ ($\chi < 0.3$). This provides a tentative working scheme for parameterizing the momentum transport to the shelf water at the shelf break. A flux scaling with $VNh^2$ is consistent with that adopted for wave drag in the atmosphere (e.g., see Palmer et al. 1986).

### *b. Is the momentum flux significant?*

The wave momentum is positive in the direction of wave propagation through the mean flow. It therefore has a positive component in a direction contrary to the mean flow that is supported by the pressure acting on the seabed. The momentum transferred back into the mean flow when waves break, or otherwise interact with the flow field to transfer their momentum to it, will therefore accelerate the fluid in a direction contrary to the mean flow over the slope generating area. This will retard the mean current where it is in the slope flow direction or possibly drive a countercurrent on the shelf. Since the internal waves reaching the shelf have a component of momentum directed in the onshelf direction, the source of which is a component of the lift forces experienced by the topography, they may also tend to drive flow onto the shelf, at least until resisted by the production of adverse pressure gradients. There are several aspects to fully parameterizing the momentum flux and its effects. These are (i) characterizing the topography, or roughness, of the continental slope, (ii) providing an estimate of the flux components of the internal waves generated by this topography and the

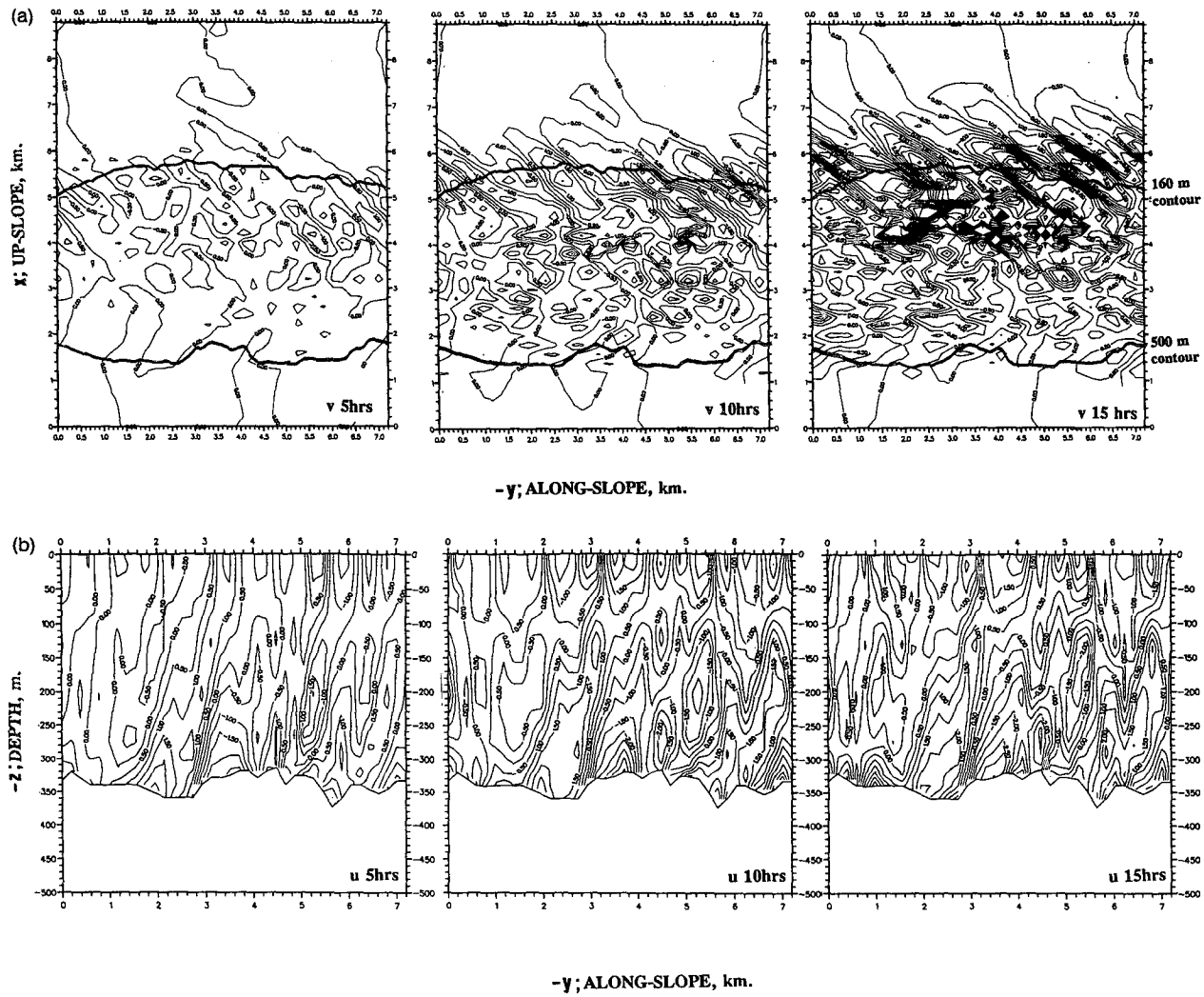


FIG. 9. Contours of (a) the across-slope $x$ component of current at the sea surface in a horizontal section extending from $x = 1.4$ km to 7.9 km and from $y = 0$ to $-7.2$ km in Fig. 8, and (b) the alongslope ($y$) current fluctuations in a vertical section at $x = 2000$ m in Fig. 8. Waves result from a uniform flow with $N = 10^{-3}$ s$^{-1}$ at speed 0.1 m s$^{-1}$ along the slope in the $y$ direction, after (left to right) 5 h, 10 h, and 15 h. Units are centimeters per second and contours are drawn at 0.5 cm s$^{-1}$ intervals. The numerical model is periodic in the $y$ dimension. A period of 15 h gives an advection distance of 5.4 km, too short to allow the disturbances generated by the topography to be advected and to recross the slope area. The lee wave patterns are stationary.

flow over it, and (iii) predicting the region where momentum in the internal wave field may be surrendered to the mean flow and the size of this local transfer. Of these, the third is possibly the most difficult to address.

Equation (11) provides an outer boundary condition for the shelf circulation. Where the momentum is surrendered to the shelf-sea circulation will depend upon the processes that lead to the transfer of stress from the waves, such as wave breaking or wave–flow interaction, and corresponding distances over which these are effective. The model does not have the resolution to address wave breaking or soliton development. Sandstrom and Elliott (1984), however, found that internal tidal waves and associated internal wave solitons observed near the shelf break are dissipated within about 10 km of the shelf break and over periods of about $5 \times 10^4$ s, with shear flow instability probably playing a part. In their analysis of other observations of internal waves propagating on the shelf, Sanford and Grant (1987) conclude that dissipation in the benthic boundary layer is unable to account for the dissipation observed; other mechanisms such as internal wave breaking must be important.

An eddy diffusion coefficient for momentum at the shelf break, $\kappa$, may be derived from the equation $\tau/\rho_0 = \kappa dU/dx$. If $dU/dx = U/\mathrm{Ro}$, where Ro is the internal

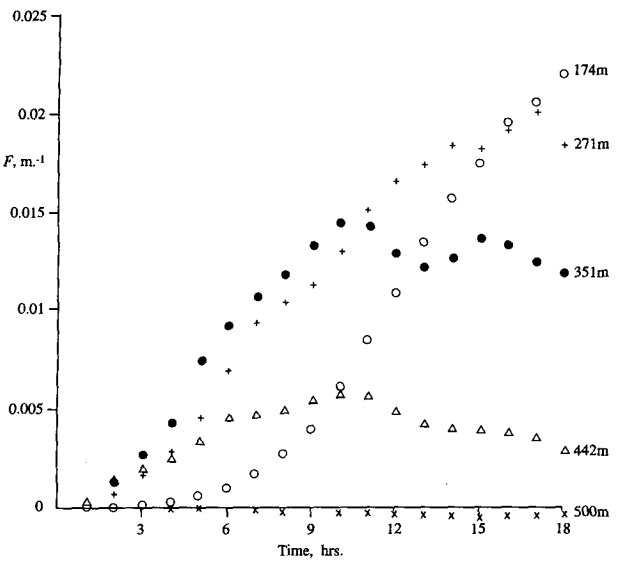


FIG. 10. The nondimensionalized upslope momentum flux $F = Fx/(h^2\rho_0 VNA)$ at 174 m (open circles), 272 m (vertical crosses), 351 m (dots), 442 m (triangles), and 500 m (diagonal crosses) water depth as a function of time after the onset of a flow with $N = 10^{-3}$ s$^{-1}$ at 0.1 m s$^{-1}$ over the topography shown in Fig. 8. Numerical instability sets in after 18 h.

Rossby radius of deformation of the shelf waters (equal to $NH/f$) and which might be supposed provides a scale for the local current field and therefore for wave–flow momentum transfer, then with $\tau = \tau_*$, $\kappa$ is equal to $kN^2h^2H/f$. The value of $\kappa$ falls to zero when $N$ tends to zero, a condition (as in winter) in which no internal waves can propagate onto the shelf. With $N = 10^{-3}$ s$^{-1}$, $f = 10^{-4}$ s$^{-1}$, $H = 200$ m, and $h = 10$ m, $\kappa = 14\ (\pm 6) \times 10^2$ m$^2$ s$^{-1}$, a large value at the scale, 20 km, of the corresponding Ro, less than the 10-km wave dissipation scale found by Sandstrom and Elliott (1984).

Alternatively the timescales associated with the rate of transport across the shelf break or the spinup of the shelf water near the shelf edge may be estimated. The former is given by the ratio of the momentum in the slope current divided by the flux. The momentum per unit alongslope length of the current is its cross-sectional area multiplied by $V\rho_0$ and, using the $s_\alpha = 0.1$ slope from 200-m depth to 1000-m depth, this is $9.6 \times 10^6 V\rho_0$ (SI units). The corresponding momentum flux is $\tau_* \times (200\text{ m}) \times (8\text{ km})$, and the timescale is $1.2 \times 10^4/kNh^2$, or $(4.9 \pm 2.1)$ days, if $N = 10^{-2}$ s$^{-1}$ and $h = 10$ m. The corresponding spinup time for a band of shelf water of width Ro = 20 km to achieve a speed of 0.1 m s$^{-1}$ is $(4.0 \pm 1.9)$ days. These times are sufficiently small for the flux to be a significant in driving the currents.

The magnitude of the stress at the shelf break can also be compared to that of the drag of the mean flow on the seabed

$$\tau_B = C_D\rho_0 V^2, \tag{12}$$

where $C_D$ is a drag coefficient, approximately equal to $3 \times 10^{-3}$ (Heathershaw 1979). The maximum momentum flux across the shelf break per unit area when $\beta = 0$ is $5 \times 10^{-2}\rho_0 h^2 VN$. With $V = 0.1$ m s$^{-1}$, this is equal to $\tau_B$ when $h = 2.5$ m for $N = 1 \times 10^{-3}$ s$^{-1}$, or $h = 0.8$ m for $N = 1 \times 10^{-2}$ s$^{-1}$. These values are smaller than the amplitude of typical topography.

## 6. Discussion

Waves of stationary phase generated in the wake of rough topography on the continental slope have been considered. It has been shown analytically that there is a preferential transfer of internal wave momentum toward shallower water even for waves that, at generation, have a component of their group velocity directed toward deeper water. The numerical estimates are consistent with the analytical conclusions. The waves will transfer momentum over the upper slope and toward shallow water, across the shelf break if stratification allows (during summer stratification), or probably into a zone of wave breaking near the intersection of the thermocline and the slope when (in winter) it does not. The fluxes appear to be large enough to play a significant role in the seasonal variability and dynamics of this region.

The area at the top of the slope appears likely to be most effective in driving the flux at the shelf break. The stress $\tau_*$ is proportional to $N$, $V$, and $h^2$, and the largest values of $N$ are generally in the thermocline near the top of the slope. The amplitude of features, and therefore $h$, is commonly largest at depths between that of the shelf break and 2000 m, becoming shrouded by sediment toward the foot of the slope. More significantly, values of $L_{\text{crit}}$, (8), are generally only a few kilometers or so, and waves generated in deep water on the slope far from the shelf break will suffer multiple reflections and consequent dissipation in the turbulent boundary layers, while waves generated near the shelf break arrive having suffered little dissipation. Moreover the small horizontal-scale topographic features required to satisfy (2), such as small canyons and rills, may "merge" with distance downslope. In consequence, the largest internal wave contributions to the momentum flux at the shelf break are usually expected to arise from close to the top of the slope.

Except in topography characterized by features leading to large Fourier components with large $|\beta|$, direct radiation of wave energy into deeper water will be small. The increasing magnitude of $N$ and $\alpha$ as waves propagate upward from the foot of the slope will lead to reflection from the slope; most of the momentum of waves generated in deeper water will be directed toward deeper water provided that the waves do not loose their momentum to the mean flow before reflection.

Those internal waves generated by a boundary current that loose their momentum by breaking while still over the slope, so contributing a drag to the alongslope current, may possibly be one of the processes contributing to flow separation from the continental slope.

The estimate of momentum transfer summarized in (11) needs to be further tested and refined, particularly in view of the simplifications made in the analysis; it is at best a working model that provides some indication of the possible importance of effects. Accurate measurements at sea are particularly difficult, given the need to resolve the relatively small cross-flow components of order 1 cm $s^{-1}$ in a mean flow of 10–20 cm $s^{-1}$ and to remove possible bias of local topography inherent in data derived from moored current meters so as to obtain reliable averages. The time and space average momentum fluxes and the scale at which the flux is carried might be estimated from acoustic Doppler current profiles from a vessel steaming repeated legs along the shelf break several times per tidal cycle. Together with reliable topographic and CTD survey and some measurements of mean currents and temperature from an array of moored current meters down the slope, this offers a means of testing or establishing a parametric estimate of the flux onto the slope and from the deep ocean.

The dependence of the internal wave stress on the size of small-scale features of topography emphasizes the pressing need to obtain better survey data of the topography of the upper slope. Further attention also needs to be given to other components of drag (see Holloway 1992).

*Acknowledgments.* The setting up and running of the program was done by Dr D. Jiang (with funding from NERC Grant GR3/8001) and Mr J. M. Keen (with funding from the EEC MAST II OMEX programme MAS2 CT93-0069). I am grateful for the support they provided. Dr M. Blackley, Proudman Oceanographic Institution, Birkenhead, U.K., kindly helped obtain the chart reproduced in Fig. 9. A early version of this paper was presented at the 'Aha Huliko'a Hawaiian Winter Workshop in January 1995.

## APPENDIX

## Oscillatory Flows with Variable $N^2$: Case Studies

The conditions of stratification and geometry of these four case studies are described in section 4c.

When $V$ (m $s^{-1}$) = 0.2 sin$\sigma t$, the condition (2) for wave generation in steady flow conditions is satisfied at 1000 m at the foot of the slope only when $0.46 < t$ (h) $< 5.54$ on the positive flow cycle ($V > 0$) and when $6.46 < t$ (h) $< 11.54$ on the negative cycle ($V < 0$). Equation (2) is satisfied at depths between 1000 m and 580 m for even more limited times. These generation conditions re-occur with 12-h periodicity. The generation condition is not satisfied at any phase in the tidal cycle at depths shallower than 644 m. The flux of momentum at the shelf break is found to be oscillatory with frequency $\sigma$ and with equal positive and negative values corresponding to fluxes of momentum in the positive and negative $y$ directions. The peak fluxes are delayed some 9 h after the maximum currents since the waves have to propagate some distance up the slope from their generation positions before arriving at the shelf break. The value of $F_1$ based on the maximum flux, $Fx_1$, the maximum flow, and the minimum $N$, is about 0.01 $m^{-1}$. That based on the mean $N$ in the wave generation zone and the rms $V$ is about 0.005 $m^{-1}$. These values are smaller than those shown in Fig. 7; some waves generated at small angles will be refracted in the $N$ gradient and will reflect from the slope, and generation is not continuous. When $V$ (m $s^{-1}$) = 0.4 sin$\sigma t$, the flux at the shelf break is again found to be periodic and symmetrical, but with phase now delayed by only 3 h; (2) is now satisfied for longer periods and over a greater depth range on the slope. Here $F_1$ based on the maximum flux, $Fx_1$, and on $V = 0.4$ m $s^{-1}$, lies between 0.042 $m^{-1}$ (using the minimum $N$) and 0.0054 $m^{-1}$ (using the maximum $N$ on the slope).

Two cases with a tidal plus a steady mean flow of 0.1 m $s^{-1}$ are examined. When $V$ (m $s^{-1}$) = 0.1 + 0.2 sin$\sigma t$, wave generation occurs at the foot of the slope with $V > 0$ when $-0.5 < t$ (h) $< 6.5$, and with $V < 0$ for the shorter period $7.6 < t$ (h) $< 10.4$. Generation with $V > 0$ extends from 1000 m up the slope to 413-m depth, but only to 878 m when $V < 0$. In consequence the flux is found to be rectified with a mean value of $F_1$ of 0.018 $m^{-1}$ based on the mean flow and maximum $N$ at generation. The direction of the flux corresponds to $V > 0$. The amplitude of the variation in the flux is about half the mean value, with peak values having a delay of 6 h after peak currents. When $V$ (m $s^{-1}$) = 0.1 + 0.4 sin$\sigma t$, the momentum flux is again strongly rectified. Fluctuations are found to lag the maximum flow by 3 h. The mean value of $F_1$ based on the mean flow and maximum $N$ at generation is 0.041 $m^{-1}$, a value comparable to those found in steady flows (Fig. 7). The amplitude of the momentum oscillations is about equal to their mean value, so varying between zero and 0.082 $m^{-1}$.

## REFERENCES

Baines, P. G., 1971a: The reflection of internal/inertial waves from bumpy surfaces. *J. Fluid Mech.*, **46,** 273–291.

——, 1971b: The reflection of internal/inertial waves from bumpy surfaces. Part 2: Split reflection and diffraction. *J. Fluid Mech.*, **49,** 113–131.

Chapman, D. C., and D. B. Haidvogel, 1993: Generation of internal lee waves trapped over a tall isolated seamount. *Geophys. Astrophys. Fluid Dyn.*, **69,** 33–54.

Eriksen, C. C., 1982: Observations of internal wave reflection off sloping bottoms. *J. Geophys. Res.*, **87,** 525–538.

Haidvogel, D. B., J. L. Wilkin, and R. Young, 1991: A semi-spectral primitive equation ocean circulation model using vertical sigma

and orthogonal curvilinear horizontal coordinates. *J. Comput. Phys.*, **94,** 151–185.

Heathershaw, A. D., 1979: The turbulent structure of the bottom boundary layer in a tidal current. *Geophys. J. Roy. Astronom. Soc.*, **58,** 395–430.

Holloway, G., 1992: Representing topographic stress for large-scale ocean models. *J. Phys. Oceanogr.*, **22,** 1033–1046.

Holmes, R., 1994: Seabed topography and other geotechnical information for the Shelf Edge Study 55°N–60°N W of Britain. British Geological Survey Tech. Rep. WB/94/15, 30 pp. + 7 maps + appendices.

Maxworthy, T., 1979: A note on the internal solitary waves produced by tidal flow over a three-dimensional topography. *J. Geophys. Res.*, **84,** 338–346.

Palmer, T. N., G. J. Shutts, and R. Swinbank, 1986: Alleviation of a systematic westerly bias in general circulation and numerical prediction models through orographic gravity wave drag parameterisation. *Quart. J. Roy. Meteor. Soc.*, **112,** 1001–1039.

Sandstrom, H., and J. A. Elliott, 1984: Internal tide and solitons on the Scotian Shelf; A nutrient pump at work. *J. Geophys. Res.*, **89**(C4), 6415–6426.

Sanford, L. P., and W. D. Grant, 1987: Dissipation of internal wave energy in the bottom boundary layer on the continental shelf. *J. Geophys. Res.*, **92**(C2), 1828–1844.

Thorpe, S. A., 1968: On the shape of progressive internal waves. *Philos. Trans. Roy. Soc. London, Ser. A,* **263,** 563–614.

——, 1992: The generation of internal waves by flow over the rough topography of a continental slope. *Proc. Roy. Soc. London, Ser. A,* **439,** 115–130.

Wunsch, C., 1971: Note on some Reynolds stress effects on internal waves on slopes. *Deep-Sea Res.*, **18,** 583–591.